Materials Today Physics 4 (2018) 28–35

Contents lists available at ScienceDirect

Materials Today Physics

journal homepage: https://www.journals.elsevier.com/materials-today-physics

Seamless modulus gradient structures for highly resilient, stretchable system integration

Zhigang Wu [a, b, *], Shuo Zhang [a], Alexey Vorobyev [b], Kristofer Gamstedt [b], Kang Wu [a], Chuanfei Guo [c], Seung Hee Jeong [a, b, **]

[a] State Key Laboratory of Digital Manufacturing Equipment and Technology, Huazhong University of Science and Technology, Luoyu Road 1037, Wuhan 430074, China
[b] Department of Engineering Sciences, The Angstrom Labortory, Uppsala University, Box 534, Uppsala 751 21, Sweden
[c] Department of Materials Science and Engineering, Southern University of Science and Technology, Shenzhen 518055, China

ARTICLE INFO

Article history:
Received 11 January 2018
Received in revised form
6 February 2018
Accepted 14 February 2018

Keywords:
Seamless modulus gradient structure
Resilience
Stretchability
System integration

ABSTRACT

Hybrid system integration of rigid components into stretchable systems is often necessary when targeting for valuable functions in various scenarios. Among them, (Young's) modulus gradient structures for system integration demonstrate excellent mechanical performance when stretched. However, the mechanical reliability is still limited under large deformation due to the inherent interface between materials of different modulus. Here, a seamless transition between heterogeneous moduli parts made with polydimethylsiloxane (PDMS)-based elastomers is presented for stretchable system integration by simply tuning their modulus via introducing a small amount of an additive into some parts of the substrate. These gradient structures not only provide a high stretchability (~250%) for the overall system, but also improve the resilience of the system (can be stretched up to 50,000 cycles from 0 to 150% global strain) at the same time. The seamless modulus gradient structures provide a simple and effective way of allowing highly resilient and stretchable system integration for various soft intelligent systems.

1. Introduction

Offering unsurpassed morphological dynamics and adaptability, soft intelligent systems with excellent mechanical compliance and stretchability of materials or structures, such as soft electronics and robotics, have shown great advantages when interacting with humans or the environment [1–3]. A few are listed here, for instance, a conformal sensor array for high resolution brain signal mapping [4], a new balloon catheter with feedback signals [5], a soft gripper that can manipulate fragile, random, and complex shaped objects [6,7], a self-driven hopping robot that can explore in complex surroundings [8], a tissue-engineered artificial ray guided by light [9], wearable silicon electronics based on system-level integration using serpentine structure [10] and an ultrathin stretchable system using polydimethylsiloxane (PDMS) suction-cup/substrate of gradual modulus [11]. To provide above mentioned vivid functions and exploit great morphological dynamics and adaptability at the same time, heterogeneous material-made rigid components including functional materials, rigid components and their assembled systems in elastomer packaging, are often necessary when implementing soft systems in the practical situations.

Several strategies enabling hybrid system integration in elastomers have been reported, for instance, thin film-based island-bridge structures [12–15], or a hybrid structure with a localized stiff cell, for which a rigid component was embedded in a thicker elastomeric package [16]. Nevertheless, heterogeneous integration systems where heterogeneous modulus occurs cause stress concentration around integrated parts, and lead to high mechanical stress at the interface between rigid parts and soft substrates when stretched [17,18]. For engineering properties in general, functional graded materials has been an active research field for decades [19], to improve the structural integrity of components. The concept of modulus gradient structure is widely found in nature to achieve

* Corresponding author. State Key Laboratory of Digital Manufacturing Equipment and Technology, Huazhong University of Science and Technology, Luoyu Road 1037, Wuhan 430074, China.
** Corresponding author.Department of Enginnering Sciences, The Angstrom Laboratory, Uppsala University, Box 534, Uppsala 751 21, Sweden.
E-mail addresses: zgwu@hust.edu.cn, Zhigang.Wu@angstrom.uu.se (Z. Wu), Seunghee.Jeong@angstrom.uu.se (S.H. Jeong).

https://doi.org/10.1016/j.mtphys.2018.02.002
2542-5293/

mechanical resilience [20–23], such as in the gradient interface tissue of living bodies [24]. Several modulus gradient structures with PDMS have been reported, either by depositing a diamond-like carbon film onto a silicone substrate through pulsed laser ablation of an isolated stiff circuit island [25], or by local tuning of mechanical properties of PDMS-made structures with a photo-inhibitor via UV light exposure [26–28]. However, the global stretchability of such systems has not been significantly improved, and delamination is a potential risk under large deformation. In addition, an out-of-plane modulus gradient structure was recently demonstrated [29].

As demonstrated above, when applying an external tensile force to a modulus gradient structure, such as an island-bridge design, different effective strains are induced in each region due to the large difference of engineering modulus between a stiff material and a soft material. The soft material region exhibits larger strain than that of the stiff region. Consequently, the resulted high stress concentration often arises at the interface between soft and stiff materials. Frequently, the interface between two materials is weaker and more prone to cracking, than the two materials independently. The stress concentration at the interface is typically higher if there is a large elastic mismatch between the two constituents [30]. Therefore, a seamless modulus gradient structure is effective to lower stress concentration and to achieve high stretchability as well as high resilience under a large deformation. Additionally, originating from the same material with very similar chemical properties, the seamless transition can act as a connection between the soft and stiff regions, thereby improving the interfacial strength and the overall stretchability.

By simply tuning modulus with a small amount of an additive (polyethylenimine ethoxylated, PEIE) in PDMS [31] and using it with a semi-cured state of PDMS [32], we present a seamless modulus gradient structure with different moduli parts, targeting highly resilient and stretchable system integration. The experimental results as well as numerical analysis for various modulus gradient structures indicate that the seamless modulus gradient greatly extends the overall stretchability compared to previous approaches, such as those in Refs. [25–28]. Furthermore, the integration of various rigid components, such as light-emitting diodes (LEDs), chips and batteries are integrated and demonstrated. It shows a stretchability up to a 250% strain, which is significantly higher than that made with homogeneous modulus PDMS (up to 80%). More importantly, a rigid component-integrated stretchable system shows great mechanical resilience under large deformation, which can be stretched over 50,000 load cycles from 0 to 150% global strain without any electrical or mechanical failures.

2. Results and discussion

As shown in Fig. 1a, we employed native PDMS (10:1 wt ratio of silicone base to curing agent in this paper) and modulus-tuned PDMS (hereafter, S3PDMS) [31] to obtain modulus gradient structures with a simple curing process. Since the S3PDMS was made from the same base of PDMS, with more compatible polymers next to one another, the base polymer chains in both PDMS and S3PDMS could be crosslinked at the interfaces and resulted in strong connections that can sustain large strain without breaking. Thus, a seamless connection between the S3PDMS and native PDMS without an obvious boundary, which is a seamless modulus gradient structure, was formed (Fig. S1).

To investigate the effective modulus and the effective strain of various combinations of different moduli, we tested samples of PDMS, S3P20, S3P30, S3P40, H20, H30 and H40 (S3P20, S3P30 and S3P40 are named for S3PDMS mixed with 20, 30 and 40 μl of PEIE, respectively. H20, H30 and H40 are named for seamless modulus gradient structures with PDMS parts and S3P20, S3P30 and S3P40 parts, respectively. The configurations of the samples are shown in Fig. S2). The maximum elongation and effective modulus of various elastomers and seamless modulus gradient structures without rigid components integration are shown in Fig. 1b. We can see that the modulus of PDMS (~2.0 MPa) is two orders of magnitude higher than the modulus of S3P40, which is ~24 kPa. Stretchability (maximum elongation at breaking) of PDMS (~100%) is less than that of S3PDMS (~300%). S3PDMS reveals both excellent mechanical stretchability and modulus tunability. Because of the stiff region (normal PDMS), the seamless modulus gradient structures (H20, H30 and H40) show smaller elongation at breaking than that of the pure ones (S3P20, S3P30 and S3P40, respectively), whereas the effective moduli are quite similar.

Moreover, we presented hybrid integration systems either with an LED or four rectifier chips having dip-type sharp connect legs (Fig. 1c and d). Both of them were stretched up to 150% under unidirectional strain and the PDMS part exhibited negligible deformation (~8%), compared to that of S3PDMS parts (~200%). The rigid components in stiff regions can be effectively protected regardless of shapes, numbers and integrated positions of the components.

To understand the stress/strain distribution of seamless modulus gradient structures, tensile tests of PDMS, S3P20, S3P30, S3P40, H20, H30 and H40 without rigid component integration were conducted (Fig. 2a and b). Because seamless modulus gradient structures included a small volume of stiff portion of PDMS, the effective moduli of H20, H30 and H40 were slightly higher than that of S3P20, S3P30 and S3P40, respectively. However, the maximum elongation of the former is smaller than that of the latter. This indicates that a hard part does not have a significant influence on compliance and stretchability of the whole system when the stiff region is small enough, compared to soft regions. Compared to the case of H40, the PDMS area between the S3P20 parts in H20 showed larger strain because the modulus difference of H20 is smaller than that of H40 (Fig. 2b).

Since the volumes are connected in series, with each part carrying the same average axial stress, a simple rule of mixtures model can be applied to estimate the overall stiffness. Considering the different moduli and volumes of a soft and a stiff region when the volume ratio of S3PDMS and PDMS is 2:1, the effective modulus of the seamless modulus gradient structure when stress is assumed homogeneous throughout the system can be expressed as [33].

$$\frac{V}{E_e} = \frac{2V_1}{E_1} + \frac{V_2}{E_2} \tag{1}$$

where E_e is the effective modulus of a modulus gradient structure, E_1 and E_2 are the moduli of the soft part and the hard part, respectively, and V_1 and V_2 are the volumes of the soft and hard part, respectively. The effective modulus can be derived as

$$E_e = \frac{E_1 E_2}{\frac{2V_1}{V}E_2 + \frac{V_2}{V}E_1} \tag{2}$$

The applied global strain is

$$\lambda_g = \frac{2\lambda_1 L_1 + \lambda_2 L_2}{2L_1 + L_2} \tag{3}$$

where L is the undeformed length, and λ is the stretch ratio. Subscripts 1 and 2 represent the soft and the hard part, respectively. By defining $\eta = L_1/L_2$, equation (3) can be expressed as

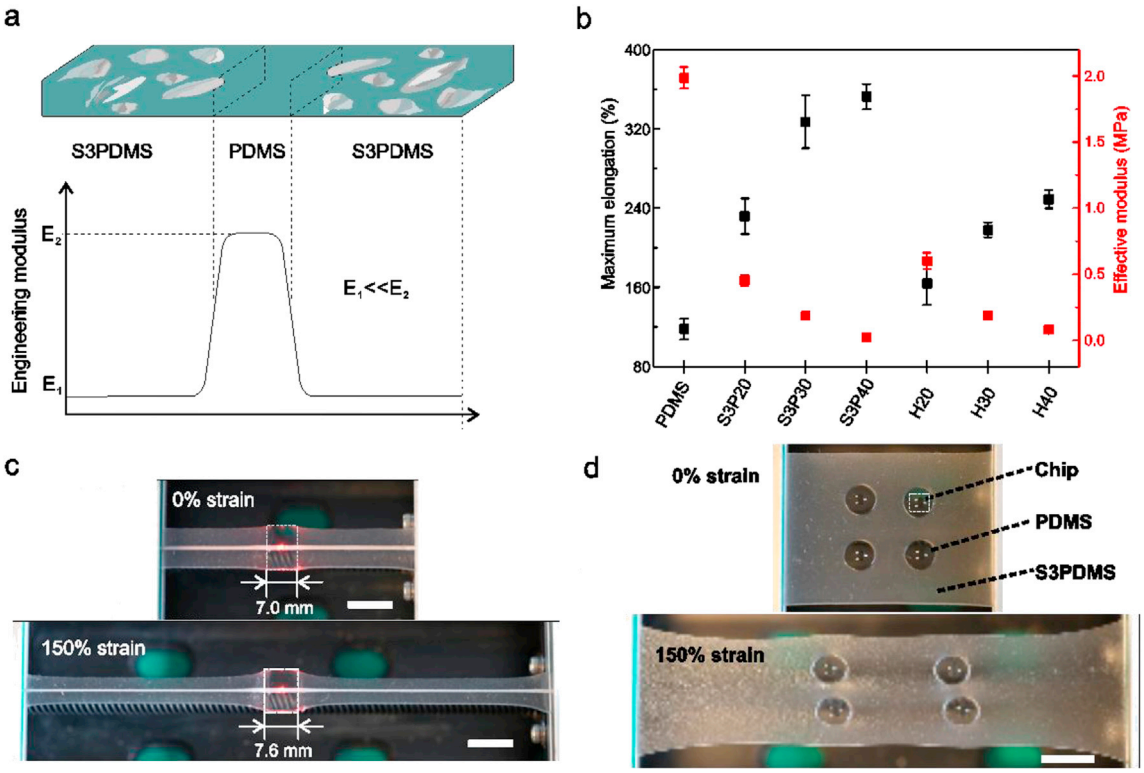

Fig. 1. Seamless modulus gradient structures made with PDMS-based elastomers (a) A conceptual drawing of a highly resilient soft and stretchable system made with a seamless modulus gradient structure. In the following experiments of this paper, the PDMS in the center region was made as 10:1 wt ratio of silicone base to curing agent. The gray areas in S3PDMS represent low-density region of crosslinking. (b) The maximum elongation and effective modulus of various elastomers and seamless modulus gradient structures without rigid components integration. The effective modulus was fitted as the slope of initial linear part of stress-strain curve. H20, H30 and H40 are sample notations for seamless modulus gradient structures that consist of PDMS and S3P20, S3P30 and S3P40 (S3PDMS prepared with 20, 30 and 40 μl PEIE). All samples (1.6 mm × 4.0 mm × 35 mm) were fully cured. (c) Photographs of uniaxial stretched H40 embedding an LED and liquid alloy conductors, and (d) four rectifier chips having dip-type sharp connect legs, which have larger volume than the LED. Scale bar indicates 10 mm.

$$\lambda_g = \frac{\lambda_1}{1+\frac{1}{2\eta}} + \frac{\lambda_2}{1+2\eta} \tag{4}$$

Furthermore, this model can be expanded to calculate the effective modulus for a multi-segmented modulus gradient structure with several soft and stiff parts.

Simulation and tensile tests were conducted to investigate the stress/strain distribution of our seamless modulus gradient structures. The tensile behavior of modulus gradient structures during stretching tests showed good agreement with simulation results under a 150% global strain (Fig. 2c). The PDMS region in H20 was stretched much more than that of H30 and H40, indicating a relative gradient difference affected to strain difference (Fig. 2d). The H20 showed the highest stress level in both the PDMS region (~1.60 MPa) and the S3P20 regions (~1.18 MPa). The H40 showed the lowest stress level in soft regions because of the highly compliant and stretchable characteristics of S3P40. The stiff part made of PDMS in H40 effectively kept at a quite small strain since the majority of deformation is in the soft parts made of S3P40 (Fig. 2e). From Fig. 2c–e, we find that the difference of stress level of PDMS part and S3PDMS part tends to be smaller when the soft part become lower modulus in H20, H30 and H40. It indicates that seamless modulus gradient structures are useful to moderate stress gradient and reduce stress concentration, even though minor stress concentration still occurs at the transition area. Ideally, with more small gradients of modulus between soft and stiff regions, stress would spread out more gently. However, our seamless modulus gradient structures exhibit a smooth transition which is similar to the smooth modulus gradient. According to the results, strain distribution at the interface between the soft and hard regions becomes smoother from H20, to H30, and to H40.

To further understand the strain behavior of each part, we measured the local strains in seamless modulus gradient structures. As shown in Fig. 2f, the local strain of each part was measured when the volume ratio of the soft part (S3PDMS) to the stiff part (PDMS) is 2:1. During the stretching test, the same global strain was applied to all samples. Local strain applied to each part was measured from photo images. The results showed that the local strain of S3PDMS and PDMS parts increase linearly with increasing applied global strain. Compared with S3P40 in H40, the local strain of the PDMS region is nearly negligible.

For the cases that rigid components were integrated in seamless modulus gradient structures, simulations and stretching tests were also conducted. As shown in Fig. 3a, the dotted line denotes that H20 would break before stretched to 150% because of highly concentrated stress (~27.5 MPa), while H40 shows the lowest stress concentration (~355 kPa) in the sharp corners of LED or the joint between S3P40 and PDMS. Therefore, we chose H40 to package LED for stretching tests. The integration systems with seamless modulus gradient structures, for instance integrated with an LED and liquid alloy circuit, were tested (Fig. 3b). The seamless modulus gradient structure (H40) enhanced the stretchability up to ~200%, compared to homogeneous modulus system integration under the same conditions (<80%). From the top view in the strain simulation, an extremely sharp strain gradient occurs at the sharp corners of the LED in both PDMS and S3PDMS packaging. It results in a high stress concentration and an abrupt change of the strain distribution. In contrast, H40 packaging systems effectively moderate this abrupt change by significant reducing the stress concentration,

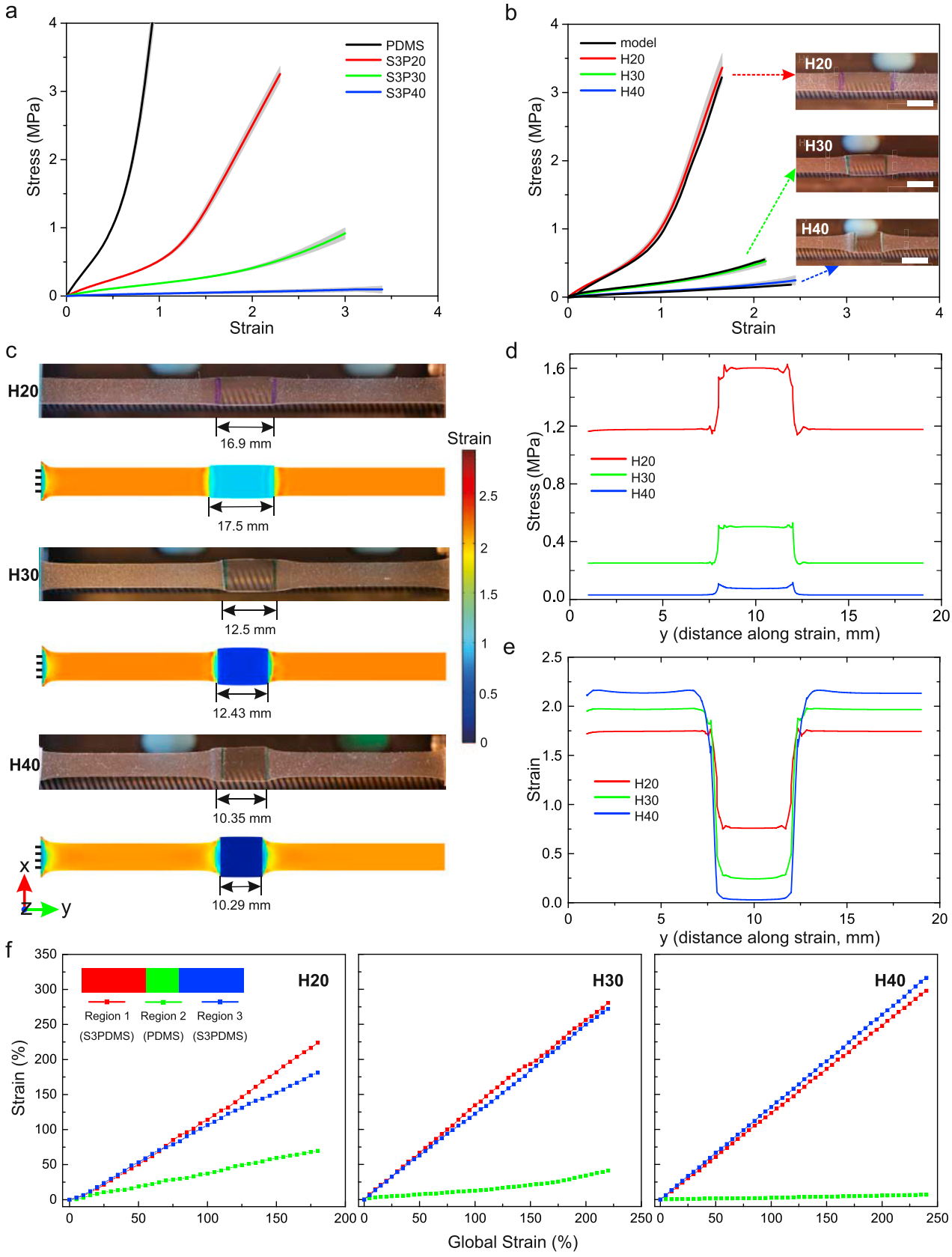

Fig. 2. Characterization of seamless modulus gradient structures without rigid components integration. Stress-strain curves of (a) pure and (b) seamless modulus gradient structures. Insets show H20, H30 and H40 under maximum strain. Theoretical model was compared with experimental data of seamless modulus gradient structures. The strain rate was 100 mm/min. Scale bars indicate 10 mm. (c–e) Strain distribution contour plots obtained from COMSOL simulation of seamless modulus gradient structures applied with a 150% global strain, and photographs of stretched samples (c). Simulated stress (d) and strain (e) values along the stretched direction are compared. (f) Local strain of each part, PDMS and S3PDMS, measured from stretching tests, according to the global strain applied to H20, H30 and H40. The inset indicates sample configurations of region 1, 2 and 3, represent S3PDMS, PDMS and S3PDMS, respectively.

which can be observed in the photographs and simulation results (strain distribution in Fig. S4).

To investigate the stretchability of rigid components (LEDs)-integrated systems with seamless modulus gradient structures (H40), the relative thickness and morphology of the side view were presented in Fig. 3c and d. During the stretching state, the thickness variation around and far-field from the LED was measured. The PDMS and the S3P40-based systems show a larger variation of the thickness (relative thickness calculated as 0.78 and 0.63, respectively) at the area around the LED than that of H40 (relative thickness calculated as 0.95), which indicates an abrupt strain distribution and a sharp strain gradient. As seen in Fig. 3d, obvious gaps occur in the PDMS sample which are not found in the H40 sample. To verify strain measurement from photograph, digital image correlation (DIC) test was employed in the case of the H40 structure with chip integration (details in Fig. S5). As shown in Fig. 3e, along the stretch direction, the stiff area integrating a rigid chip in the H40 structure was not much stretched compared to the PDMS-encapsulated structure under the same stretch condition. That means the stress concentration around the rigid chip was avoided by the seamless modulus gradient structure. According to a previous study [34], once a crack or any delimitation of the elastomer from the rigid components is initiated, the crack at the corner tends to propagate throughout elastomeric materials, which then leads to a mechanical failure. As shown in Fig. 4a and b, the applied strains showed the maximum elongation when samples were broken. When systems integrated in PDMS and S3P40, the samples were broken at the interface between LED and elastomers because of stress concentration. When systems integrated in H40, the samples were broken at soft regions. Due to the seamless connection, the transition area in H40 is strong enough to support the whole system, while the breaking always occurred at the soft region (S3P40).

When integration systems were packaged by PDMS and S3P40 elastomers, a fillet shape was generated by the large thickness variation between non-stretchable (rigid component) and stretchable parts (elastomer) under large deformation (Fig. 3d). The fillet shape resulted in a sharp strain gradient at the interface between LEDs and elastomers [35]. Hence, stress concentration was exerted, which is considerably larger than that of far-field areas. With seamless modulus gradient structures (H40), the stiff region (PDMS) with rigid components was well protected due to low strain and low stress. Compared to the obviously stress (strain) concentration between heterogeneous rigidity, the distribution of stress (strain) around the transition area became smooth when seamless modulus structures were applied. Therefore, via seamless modulus gradient structures (H40), the whole integrating system can sustain at large deformation.

To verify the enhancement of mechanical performance with the new integration strategy, several applications were demonstrated (Fig. 5). The stretchable systems with smaller LED (0603, 1.60 mm × 0.80 mm × 0.40 mm, red) and larger LED (1206, 3.20 mm × 1.60 mm × 0.55 mm, red) integration could be stretched over 50,000 cycles under 150% global strain without any mechanical or electrical failures. And the resistance changes in Fig. 5a were mainly induced by strains of liquid alloy embedded in S3P40 parts. That were ~10 Ω for smaller LED-integrated system with the original resistance of ~55 Ω and ~26 Ω for larger LED-integrated system with the original resistance of ~527 Ω. The result showed an excellent fatigue resistance of the stretchable systems. This integration can also be extended to different shapes and sizes of rigid components, for example a heat flux sensor (4.4 mm × 4.4 mm, 0.5 mm thickness), a PCB module (10.2 mm × 22.9 mm, 2.6 mm thickness), and a coin battery (2.40 mm diameter, 5.55 mm thickness), in an H40 structure at a deformation up to 150% (Fig. 5b). The multi-components-integrated system is potential for intelligent tactile sensor on mimicking human skin [36]. In Fig. 5c, a strain sensor made of liquid alloy conductors was embedded in the stiff part. We observed a small variation of resistance (<10%) and a symmetric curve indicating good protection for the hard region (PDMS) and good resilience for the integrated system. Such a strategy opens a new approach to isolate morphological deformation from external environments even for soft materials, e.g. liquid metal.

3. Experimental section

In the following experiments of this paper, a PDMS (Sylgard 184, Dow Corning) mixture was prepared with a weight ratio of 10:1 (silicone base to curing agent), and the PEIE (polyethylenimine, 80% ethoxylated solution 35–40 wt% in H_2O, M.W. = 70,000, Sigma-Aldrich) additive was handled with a pipette (10–100 μl, Eppendorf). S3PDMS mixtures (S3P20, S3P30 and S3P40) were prepared by mixing PDMS (10 g: 1 g) and PEIE (20 μl, 30 μl and 40 μl). Then, the mixtures were manually stirred with a glass rod for 1 min, followed by degassing in a vacuum chamber for 10 min. Seamless modulus gradient structures were fabricated with PDMS and S3PDMS from the same batch of mixture. PDMS-made solid spacers between different parts were inserted to keep them separated. After removing the spacers, the edges between PDMS and S3PDMS were connected and merged, and afterwards, diffused during curing (Fig. S1a). For controlling the dimension of each part in the structures, a syringe was used to measure the amount of each prepolymer by calculation of the volume. The fabricated structures were cured for 3 h at 90 °C in an oven. For fabrication of rigid component-integrated systems, a layer-by-layer process was conducted with semi-cured elastomer layers, controlled by curing temperature and time according to thickness of each layer, as shown in Fig. S3.

Tensile tests of PDMS, S3PDMS and modulus gradient structures (H20, H30 and H40) were conducted with a universal tensile test instrument (1 kN, 5944, Instron, America) at the condition of a strain rate of 100 mm/min at room temperature. Specimens were cut into a dog bone shape with a scalpel. The full displacement field on the surface of the specimens was measured with the DIC equipment (Aramis stereo system 5 M, GOM). The distance to the measured object was set to 31 cm, which gave a 34 × 29 mm^2 field of view. Each surface of the specimens was spray-painted with speckles for better contrast. The applied force values were sent from the tensile tester to the DIC system and continuously stored during testing together with the sampled images. The measurement sampling frequency was 2 Hz. Every frame that was recorded by the DIC system was compared with the original state in order to calculate the displacement and strain fields.

To measure local strain of each part of seamless modulus gradient structures (Fig. 2g) and to assess the maximum strain (stretchability) of hybrid integration systems (Fig. 3b), stretching tests were conducted by using a linear stage (A-LSQ, Zaber Technologies). The stretched length was measured by ImageJ from digital camera images. To fabricate an LED-integrated liquid alloy (Galinstan, 68.5% Ga, 21.5% In, and 10% Sn, Geratherm Medical AG, Germany) circuit, previously developed patterning technique was employed [32]. Resistance was measured with a multi-meter (34405 A, Agilent Technologies).

To characterize the mechanical and electrical stability of LED (element 14, Farnell)-integrated modulus gradient integration systems, cycling tests were conducted at a frequency of 0.2 Hz using a dynamic test instrument (E1000, Instron, America), and resistance change was measured with a multimeter (34461 A, Keysight Technologies).

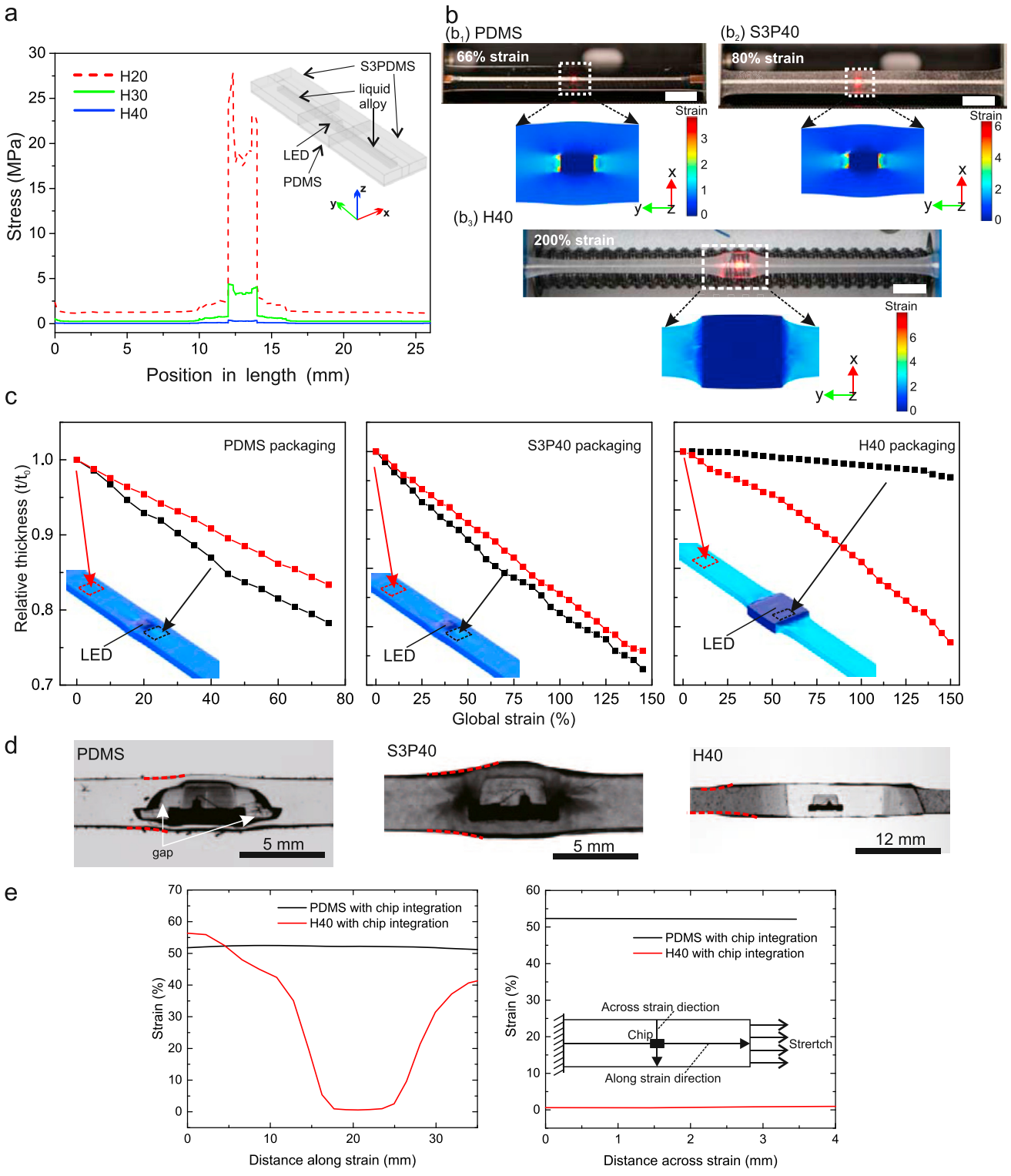

Fig. 3. Characterization of LED-integrated systems with seamless modulus gradient structures. (a) Stress distribution around integrated LED and liquid alloy conductors in seamless modulus gradient structures under a 150% global strain (The simulation results of strain distribution are shown in Fig. S4). (b) Photographs of stretched samples under maximum strain conditions. The original length of the samples was 50 mm (PDMS, S3P40 and H40). Scale bars indicate 10 mm. (c) Relative thickness measured at the area around LED (black plots) and the far-field area from LED (red plots) of integrating systems packaged in PDMS, S3P40 and H40 under applied global strain. Specifically, in H40 packaging, LED was embedded in PDMS (the middle blue part) which was not stretched much during stretching test. (d) The morphology at the side view of the integration systems packaged by PDMS, S3P40 and H40. (e) Strain distribution around LED integration in the H40 and PDMS encapsulation under 54% applied global strain, which was measured by digital camera images and DIC tests. (For interpretation of the references to colour in this figure legend, the reader is referred to the Web version of this article.)

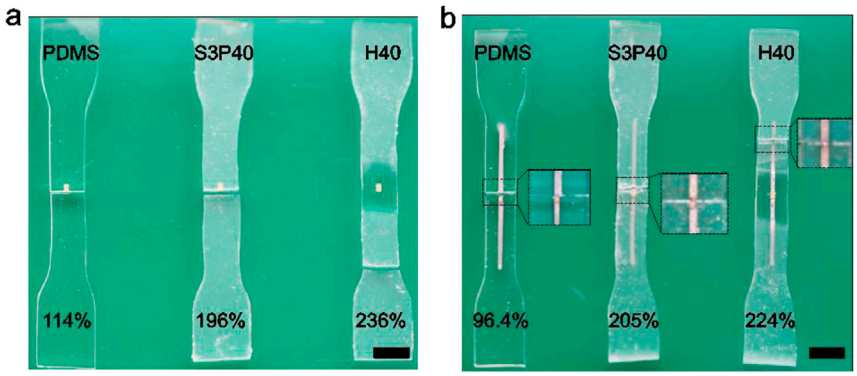

Fig. 4. Broken samples in stretching test of PDMS, S3P40 and H40 integrating with (a) LED and (b) LED connected with liquid alloy. The applied strains showed the maximum elongation when samples were broken, which are 114% for PDMS with LED, 196% for S3P40 with LED, 236% for H40 with LED, 96.4% for PDMS with LED and liquid alloy, 205% for S3P40 with LED and liquid alloy and 224% for H40 with LED and liquid alloy. Scale bars indicate 5 mm.

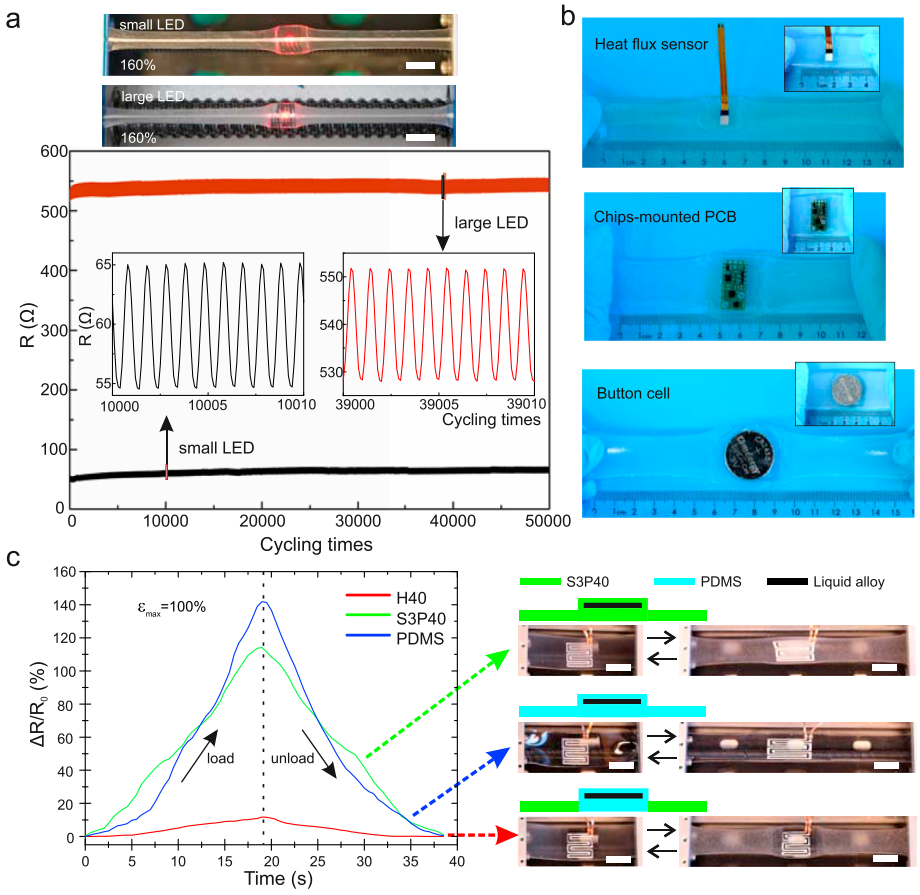

Fig. 5. Electrical characterization and case studies of highly resilient soft and stretchable systems (a) Cyclic tensile test of LED (1.60 mm × 0.80 mm × 0.40 mm and 3.20 mm × 1.60 mm × 0.55 mm)-integrated structures at a strain rate of 9 mm/s. Scale bars indicate 10 mm. (b) Various heterogeneous system integration in seamless modulus gradient structures (H40), which are stretched to 250, 200 and 150% from the top. (c) Resistance changes of liquid alloy conductors encapsulated in S3PDMS, PDMS and H40 at a stoke rate of 1 mm/s. Scale bars indicate 20 mm.

Finite element analysis based on the three parameters Mooney-Rivlin hyperelastic model were conducted using COMSOL (Multiphysics 5.1, Sweden). The least square method was used for parameters of the model in Fig. S6 and Table S1.

4. Summary

For highly resilient and stretchable system integration, a seamless modulus gradient structure with PDMS-based elastomers was developed. By adjusting stretchability and compliance of several combinations of PDMS and S3PDMS, we were able to tune the effective modulus and global stretchability. Through simulations and experiments, the stiff region (PDMS) remains relatively unstretched (strain <8%) with low stress concentration around rigid components while the soft regions (S3PDMS) take over large strain (>300%) during stretching. Stress (strain) dissipation through modulus gradient structures realizing moderate changes of stress (strain) at interface rather than tremendous change within a small

region. The results show that integration systems with seamless modulus gradient structures provide high stretchability (~250%) and good mechanical and electrical resilience (50,000 times of stretching-releasing test under 150% strain). Moreover, various rigid components-integrated systems in seamless modulus gradient structures also exhibit mechanical resilience and high stretchability under large deformation, providing potential for introducing more functions in soft intelligent systems with components integration.

Acknowledgements

We acknowledge National Natural Science Foundation of China (No. U1613204) and (No. 51575216), Pearl River Talents Recruitment Program (2016ZT06G587). Wu and Guo thank the support from Chinese central government through its Thousand Youth Talents program.

Appendix A. Supplementary data

Supplementary data related to this chapter can be found at https://doi.org/10.1016/j.mtphys.2018.02.002.

References

[1] J.A. Rogers, T. Someya, Y. Huang, Materials and mechanics for stretchable electronics, Science 327 (2010) 1603–1607.
[2] S. Kim, C. Laschi, B. Trimmer, Soft robotics: a bioinspired evolution in robotics, Trends Biotechnol. 31 (2013) 287–294.
[3] D. Rus, M.T. Tolley, Design, fabrication and control of soft robots, Nature 521 (2015) 467–475.
[4] J. Viventi, D.-H. Kim, J.D. Moss, Y.-S. Kim, J.A. Blanco, N. Annetta, A. Hicks, J. Xiao, Y. Huang, D.J. Callans, J.A. Rogers, B. Litt, A conformal, bio-interfaced class of silicon electronics for mapping cardiac electrophysiology, Sci. Transl. Med. 2 (2010), 24ra22.
[5] D.-H. Kim, N. Lu, R. Ghaffari, Y.-S. Kim, S.P. Lee, L. Xu, J. Wu, R.-H. Kim, J. Song, Z. Liu, J. Viventi, B. de Graff, B. Elolampi, M. Mansour, M.J. Slepian, S. Hwang, J.D. Moss, S.-M. Won, Y. Huang, B. Litt, J.A. Rogers, Materials for multifunctional balloon catheters with capabilities in cardiac electrophysiological mapping and ablation therapy, Nat. Mater. 10 (2011) 316–323.
[6] F. Ilievski, A.D. Mazzeo, R.F. Shepherd, X. Chen, G.M. Whitesides, Soft robotics for chemists, Angew. Chem. Int. Ed. 50 (2011) 1890–1895.
[7] R.V. Martinez, J.L. Branch, C.R. Fish, L. Jin, R.F. Shepherd, R.M.D. Nunes, Z. Suo, G.M. Whitesides, Robotic tentacles with three-dimensional mobility based on flexible elastomers, Adv. Mater. 25 (2013) 205–212.
[8] N.W. Bartlett, M.T. Tolley, J.T.B. Overvelde, J.C. Weaver, B. Mosadegh, K. Bertoldi, G.M. Whitesides, R.J. Wood, A 3D-printed, functionally graded soft robot powered by combustion, Science 349 (2015) 161–165.
[9] S.-J. Park, M. Gazzola, K.S. Park, S. Park, V. Di Santo, E.L. Blevins, J.U. Lind, P.H. Campbell, S. Dauth, A.K. Capulli, F.S. Pasqualini, S. Ahn, A. Cho, H. Yuan, B.M. Maoz, R. Vijaykumar, J.-W. Choi, K. Deisseroth, G.V. Lauder, L. Mahadevan, K.K. Parker, Phototactic guidance of a tissue-engineered soft-robotic ray, Science 353 (2016) 158–162.
[10] J. Kim, D. Son, M. Lee, C. Song, J.K. Song, J.H. Koo, D.J. Lee, H.J. Shim, J.H. Kim, M. Lee, T. Hyeon, D.H. Kim, A wearable multiplexed silicon nonvolatile memory array using nanocrystal charge confinement, Sci. Adv. 2 (2016) e1501101.
[11] M.K. Choi, O.K. Park, C. Choi, S. Qiao, R. Ghaffari, J. Kim, D.J. Lee, M. Kim, W. Hyun, S.J. Kim, H.J. Hwang, S.-H. Kwon, T. Hyeon, N. Lu, D.-H. Kim, Cephalopod-inspired miniaturized suction cups for smart medical skin, Adv. Healthcare Mater. 5 (2015) 80–87.
[12] S.P. Lacour, J. Jones, S. Wagner, L. Teng, S. Zhigang, Stretchable interconnects for elastic electronic surfaces, Proc. IEEE 93 (2005) 1459–1467.
[13] S. Wagner, S.P. Lacour, J. Jones, P.-h.I. Hsu, J.C. Sturm, T. Li, Z. Suo, Electronic skin: architecture and components, Physica E 25 (2004) 326–334.
[14] R. Vieroth, T. Loher, M. Seckel, C. Dils, C. Kallmayer, A. Ostmann, H. Reichl, Stretchable circuit board technology and application, in: International Symposium on Wearable Computers, 2009, pp. 33–36.
[15] M. Gonzalez, F. Axisa, M.V. Bulcke, D. Brosteaux, B. Vandevelde, J. Vanfleteren, Design of metal interconnects for stretchable electronic circuits, Microelectron. Reliab. 48 (2008) 825–832.
[16] S. Cheng, Z. Wu, Microfluidic stretchable RF electronics, Lab a Chip 10 (2010) 3227–3234.
[17] D.-H. Kim, Z. Liu, Y.-S. Kim, J. Wu, J. Song, H.-S. Kim, Y. Huang, K.-C. Hwang, Y. Zhang, J.A. Rogers, Optimized structural designs for stretchable silicon integrated circuits, Small 5 (2009) 2841–2847.
[18] N. Lu, Z. Suo, J.J. Vlassak, The effect of film thickness on the failure strain of polymer-supported metal films, Acta Mater. 58 (2010) 1679–1687.
[19] B. Kieback, A. Neubrand, H. Riedel, Processing techniques for functionally graded materials, Mater. Sci. Eng., A 362 (2003) 81–105.
[20] H. Chai, J.J.W. Lee, P.J. Constantino, P.W. Lucas, B.R. Lawn, Remarkable resilience of teeth, Proc. Natl Acad. Sci. 106 (2009) 7289–7293.
[21] V. Imbeni, J.J. Kruzic, G.W. Marshall, S.J. Marshall, R.O. Ritchie, The dentin-enamel junction and the fracture of human teeth, Nat. Mater. 4 (2005) 229–232.
[22] J.H. Waite, E. Vaccaro, C. Sun, J.M. Lucas, Elastomeric gradients: a hedge against stress concentration in marine holdfasts? Phil. Trans. Roy. Soc. Lond. B 357 (2002) 143–153.
[23] P. Fratzl, R. Weinkamer, Nature's hierarchical materials, Prog. Mater. Sci. 52 (2007) 1263–1334.
[24] A. Seidi, M. Ramalingam, I. Elloumi-Hannachi, S. Ostrovidov, A. Khademhosseini, Gradient biomaterials for soft-to-hard interface tissue engineering, Acta Biomater. 7 (2011) 1441–1451.
[25] S.P. Lacour, S. Wagner, R.J. Narayan, T. Li, Z. Suo, Stiff subcircuit islands of diamond like carbon for stretchable electronics, J. Appl. Phys. 100 (2006), 014913.
[26] D.P.J. Cotton, A. Popel, I.M. Graz, S.P. Lacour, Photopatterning the mechanical properties of polydimethylsiloxane films, J. Appl. Phys. 109 (2011), 054905.
[27] S.P. Lacour, I. Graz, D. Cotton, S. Bauer, S. Wagner, Elastic components for prosthetic skin, Conf. Proc. IEEE Eng. Med. Biol. Soc. (2011) 8373–8376.
[28] A. Romeo, S.P. Lacour, Concurrent photopatterning of elastic modulus and structures in photosensitive silicone elastomers, Extreme Mech. Lett. 3 (2015) 1–7.
[29] R. Libanori, R.M. Erb, A. Reiser, H. Le Ferrand, M.J. Süess, R. Spolenak, A.R. Studart, Stretchable heterogeneous composites with extreme mechanical gradients, Nat. Commun. 3 (2012) 1265.
[30] S.Y. Fu, X.Q. Feng, B. Lauke, Y.W. Mai, Effects of particle size, particle/matrix interface adhesion and particle loading on mechanical properties of particulate–polymer composites, Compos. B Eng. 39 (2008) 933–961.
[31] S.H. Jeong, S. Zhang, K. Hjort, J. Hilborn, Z. Wu, PDMS-Based elastomer tuned soft, stretchable, and sticky for epidermal electronics, Adv. Mater. 28 (2016) 5830–5836.
[32] S.H. Jeong, K. Hjort, Z. Wu, Tape transfer atomization patterning of liquid alloys for microfluidic stretchable wireless power transfer, Sci. Rep. 5 (2015) 8419.
[33] R.M. Jones, Mechanics of Composite Materials, Scripta Book Company, Washington, DC, 1975.
[34] C.Y. Hui, A. Jagota, S.J. Bennison, J.D. Londono, Crack blunting and the strength of soft elastic solids, Proc. Roy. Soc. Lond. A 459 (2003) 1489–1516.
[35] H.F. Hardrath, L. Ohman, A study of elastic and plastic stress concentration factors due to notches and fillets in flat plates, NACA report (1953) 1117.
[36] Y. Wan, Y. Wang, C.F. Guo, Recent progresses on flexible tactile sensors, Mater. Today Phys. 1 (2017) 61–73.